In vivo photoacoustic molecular imaging with simultaneous multiple selective targeting using antibody-conjugated gold nanorods

Pai-Chi Li[1, 2], Dar-Bin Shieh[3], Churng-Ren Chris Wang[4], Chen-Wei Wei[2], Chao-Kang Liao[2], Ann-Ann Ding[3], Ya-Na Wu[3], Carolina Poe[4] and Suwen Jhan[4]

Institute of Biomedical Electronics and Bioinformatics, National Taiwan University, Taipei, Taiwan
[2]Department of Electrical Engineering, National Taiwan University, Taipei, Taiwan
[3]Institute of Oral Medicine, National Cheng-Kung University, Tainan, Taiwan
[4]Department of Chemistry and Biochemistry, National Chung-Cheng University, Chia-Yi, Taiwan

Abstract

The use of gold nanorods for photoacoustic molecular imaging *in vivo* with simultaneous multiple selective targeting is reported. The extravasation of multiple molecular probes is demonstrated, and used to probe molecular information of cancer cells. This technique allows molecular profiles representing tumor characteristics to be obtained and a heterogeneous population of cancer cells in a lesion to be determined. The results also show that the image contrast can be enhanced by using a mixture of different molecular probes. In this study, HER2, EGFR, and CXCR4 were chosen as the primary target molecules for examining two types of cancer cells, OECM1 and Cal27. OECM1 cells overexpressed HER2 but exhibited a low expression of EGFR, while Cal27 cells showed the opposite expression profile. Single and double targeting resulted in signal enhancements of up to 3 dB and up to 5 dB, respectively, and hence has potential in improving cancer diagnoses.

Introduction

Molecular imaging refers to remote sensing the characteristics of biological process and interactions between molecules at the molecular level[1]. It has a great potential for the early detection and more effective treatment of diseases, because aberrations at the cellular and molecular levels occur much earlier than anatomic changes. In general, specific targeting employs an exogenous nanoprobe that has a high affinity to the molecule (i.e., the biomarker) associated with a specific type of disease, with the targeting of probes tracked using a suitable imaging system. Molecular imaging methods have developed for many different imaging modalities[1], including optical imaging[2], ultrasonic imaging[3], magnetic resonance imaging[4], and nuclear medicine based imaging[5].

The goal of targeting cancer cells is to determine the expressions of oncogenic surface molecules, which will aid the prediction of clinical outcomes and treatment responses. For this it is necessary to image cancer lesions and obtain pathogenic information on them at the molecular level. However, most previous researches reported in the literature have employed only a single target. Therefore, the goal of this study was to realize *in vivo* photoacoustic (PA) imaging with simultaneous multiple selective targeting for cancer diagnosis. We have previously demonstrated *in vitro* multiple targeting[6], and the present study further demonstrates the *in vivo* imaging of small-animal models and extravasation of multiple molecular probes.

PA imaging is a new imaging modality under preclinical development that has been applied to several biomedical applications for obtaining anatomic and functional information, including breast tumor detection[7], epidermal melanin measurements[8], blood oxygenation monitoring[9], and quantitative blood flow estimation[10]. In the current study, cylindrical antibody-conjugated gold nanorods (AuNRs) were used as nanoprobes for PA imaging to achieve multiple selective targeting. The wavelength at which the optical absorption of gold nanorods is maximal increases with their aspect ratio[11], and AuNRs with different aspect ratios can be conjugated to different antibodies and detected by irradiation with laser pulses at appropriate wavelengths.

To achieve simultaneous multiple targeting, different antibodies and a blocker (PEG) are conjugated to AuNRs with different aspect ratios to form various types of nanoprobes that are injected into blood vessels at the same time. The purpose of attaching blockers is to avoid nonspecific binding such as electrostatic binding and endocytosis[12]. The extravasating nanoprobes can target cancer cells with antigens specific to the conjugated antibody. Consequently, different types of cancer cells can be recognized and multiple characteristics can be obtained with laser irradiation at wavelengths corresponding to the peak absorption wavelengths of the nanoprobes.

The first part of this study used oral cancer OECM1 (oral squamous cell carcinoma) cells with HER2 (human epidermal growth factor receptor 2) overexpressed on the cell surface, and Cal27 (squamous cell carcinoma) cells with EGFR (epidermal growth factor receptor) overexpressed on the cell surface. These two cell types, each with a specific cell–antibody pair, were adopted to demonstrate multiple selective targeting.

HER2 expression is associated with growth characteristics and sensitivity to Herceptin chemotherapy, and is a member of the HER tyrosine kinase family that regulates cell growth and proliferation. HER2 has been associated with an aggressive phenotype and a poor prognosis, making it an appealing therapeutic target[13].

EGFR expression is strongly correlated with tumor metastasis. It is overexpressed in several epithelial malignancies, including head and neck squamous cell carcinoma (HNSCC), with 90% of such tumors exhibiting EGFR overexpression. EGFR plays a critical role in HNSCC growth, invasion, metastasis, and angiogenesis[14].

The second part of the study involved targeting two specific targets in an oral cancer cell line. The specific recognition of the antigens of CXCR4 (CXC-chemokine receptor 4) on the two selected cell types was verified carefully by Western blot analysis. CXCR4 is highly expressed in tumor cells and plays an important role in tumor metastasis[15]. It also functions as a coreceptor for human immunodeficiency virus (HIV) and is an attractive target for the development of anti-HIV drugs[16].

We conducted multiple-target measurements on OECM1 cells using HER2- and CXCR4-based nanoprobes in order to cross-examine the types and amounts of protein expressed.

To demonstrate multiple targeting, three types of nanoprobes were prepared: $AuNR_{785}$-HER2, $AuNR_{1000}$-EGFR, and $AuNR_{785}$-CXCR4; where the subscripts represent the peak absorption wavelengths of two types of gold nanorods with mean aspect ratios of 3.7 (785 nm) and 5.9 (1000 nm) (Fig. 1). The conjugated antibodies were HER2, EFGR, and CXCR4.

Results

Western blot analysis

Western blot analysis can detect and indicate the size of specific proteins in a mixture. For multiple-target molecular PA imaging, the cancer cell-line bank has been screened for appropriate model cells (see Supplementary Fig. 1). OECM1 cells overexpressed HER2 and exhibited a relatively low expression of EGFR, while Cal27 cells showed the opposite expression profile. Both cells exhibited high expressions of CXCR4.

Binding between cells and nanoprobes

The efficacy of the binding between cells and nanoprobes was examined using transmission electron microscopy (TEM). The TEM image (see Supplementary Fig. 2) of an OECM1 cell slice shows bioconjugated gold nanorods attached to the cell surface, demonstrating the specific binding ability of nanoprobes.

In vitro PA measurements of cell cultures

Before performing *in vivo* animal experiments, *in vitro* experiments with cell cultures were performed to verify the targeting ability of the bioconjugated gold nanorods to cancer cells. The samples were placed in a phantom made from transparent plastic (Rexolite 1422, San Diego Plastics,

CA). The phantom was 4 cm × 4 cm × 3 cm in size and contained several tubes with an internal diameter of 2.5 mm.

For each cell line, the cells on the left, middle, and right in the phantom were reacted with probes of a specific targeting relation (experimental group), with probes of a nonspecific targeting relation (control group), and with pure gold nanorods (control group) (see Supplementary Fig. 3).

To demonstrate multiple targeting of bioconjugated gold nanorods, the two wavelengths chosen to irradiate the samples for generating PA signals (one close to and the other far from the peak absorption of the specific target probes) were 800 and 1064 nm, corresponding to the peak absorption wavelengths of the $AuNR_{785}$-HER2 and $AuNR_{1000}$-EGFR probes. Results showed that the image intensities of the experimental groups were generally about 10 dB higher than those in the control groups (see Supplementary Fig. 4). In other words, the targeting ability of specific probes to cancer cells and the wavelength selectivity of PA detection are clearly demonstrated.

PA system for *in vivo* imaging of multiple selective targeting

The PA experimental setup for *in vivo* imaging (Fig. 2) consisted of an optical irradiating system, a precision translation stage, a homemade animal stage, and a data acquisition card. The nanoprobes and gold nanorods (control group) were injected into the tail veins of two mice. In each mouse the targeting process was monitored at multiple time points within 24 hours after probe/nanorod injection. At each measurement time point, the tumor was imaged in three cross sections to calculate the averaged PA intensity within the tumor region. After each PA scanning procedure, an ultrasound image was also acquired in the same region to show anatomic information. Ultrasound images displayed on a grayscale were superimposed with the corresponding PA images displayed in red pseudocolor.

Cal27 tumor with EGFR-probe targeting

The PA images of a Cal27 tumor for injections with $AuNR_{1000}$ and $AuNR_{1000}$-EGFR in Fig. 3 demonstrate the specific targeting ability of the $AuNR_{1000}$-EGFR probe. The contrast is higher for

the $AuNR_{1000}$-EGFR data postinjection (7 hours after injection) PA image within the tumor region (Fig. 3d) than for the preinjection image (Fig. 3c), while there is no apparent difference between the pre- and postinjection images for the $AuNR_{1000}$ injection (Fig. 3a, b). The intensities of three cross-sectional PA images of the tumor region were averaged and normalized relative to the preinjection averaged intensity of the tumor region in order to quantitatively measure the targeting efficacy. The contrast between the experimental group ($AuNR_{1000}$-EGFR injection) and the control group ($AuNR_{1000}$ injection) was maximally about 3.5 dB at 7 hours after the injection, indicating the specific targeting of $AuNR_{1000}$-EGFR to Cal27 cells. The increased intensities at 1 hour postinjection in both cases might indicate nonspecific binding due to accumulation in the circulation[17].

OECM1 tumor with HER2 probe and mixed-probe targeting

The PA images of OECM1 tumors in Fig. 4a–d also demonstrate the other specific cell–antibody binding relations. The pre- and postinjection images of the control group (i.e., injection of $AuNR_{785}$) showed no obvious changes in signal intensity (Fig. 4a, b). In contrast, the postinjection image for $AuNR_{785}$-HER2 exhibited an evident increased PA intensity relative to the preinjection image.

Multiple targeting of an OECM1 tumor with $AuNR_{785}$-HER2 and $AuNR_{785}$-CXCR4 injections revealed an enhanced contrast between the tumor region and surrounding tissues, demonstrating the effectiveness of using a mixture of different nanoprobes (Fig. 4f). Injecting mixtures with different probes yielded conspicuous PA signals from the increased level of targeted probes in the tumor region, with various protein expressions being obtained.

Fig. 4g shows normalized averaged image intensities within the OECM1 tumor regions plotted as a function of the observation time. The intensity contrast between the tumor with $AuNR_{785}$-HER2 injection (dashed line) and the tumor with $AuNR_{785}$ injection (dotted line) was up to about 2 dB at 14 hours, while multiple targeting with $AuNR_{785}$-HER2 and $AuNR_{785}$-CXCR4 showed maximum contrasts of 4 dB at 10 hours and 3 dB at 24 hours.

Discussion

Biocompatibility has been an important issue for *in vivo* applications of gold nanoparticles. Results from analyses of AuNRs including *in vitro* biosafety tests (see Supplementary Fig. 5), hemocompatibility analyses (see Supplementary Fig. 6) and *in vivo* systemic toxicity tests (see Supplementary Fig. 7) show that AuNRs are biocompatible and hemocompatible for *in vivo* tests. Nanoparticles exhibit satisfactory biosafety at the dosages expected for *in vivo* applications. The results of an *in vivo* toxicity test for AuNRs administered to BALB/c mice via tail-vein injection were also satisfactory, with all mice surviving the 2-month observation period.

In addition, the temporal biodistribution of AuNRs in BALB/c mice was analyzed to determine their metabolic clearance. An evaluation of metabolic uptake and clearance of the nanoparticles indicated that these nanoparticles were mainly taken up by the liver, and the accumulations in the spleen and liver reached a plateau at 24 hours then gradually reduced over time (Fig. 5). The nanorod concentration returned to the background level at 168 hours after the intravenous injection.

The biodistribution of particles from organs removed at 24 hours postinjection indicated that the percentage concentrations of particles relative to the injected dose for the injections with $AuNR_{785}$-HER2 and $AuNR_{785}$ were 8.88% and 6.1% (Fig. 6), which indicates a 3.26-dB difference compared to 2 dB in the imaging results. The contrast could be improved by determining the optimal strategy for conjugating antibodies and PEG to increase the targeting efficiency and to avoid nonspecific binding. Below we describe how to titrate the appropriate concentration of nanoprobes or other types of conjugated targeting probes to enhance the PA signals.

PA molecular imaging with multiple selective targeting has been demonstrated using AuNRs on oral cancer cells *in vivo*. The results reveal that information about the oncogene surface molecules of cancer cells can be obtained with PA techniques, which will help to improve our understanding of cancer cells better and to develop effective diagnosis tools as well as indications for effective treatments. Safe and effective gold-nanoparticle-based cancer diagnoses have great potential in the pharmaceutical industry and could also make significant contributions in the biomedical field.

Acknowledgments

Financial supports from the National Science Council, the National Health Research Institutes, NTU Center for Genomic Medicine, and the NTU Nano Center for Science and Technology are gratefully acknowledged.

Author contributions

P. L. designed the experiments and wrote the paper. D. S. provided the antigens/antibodies, *in vitro/in vivo* tumor models and associated assays, performed biocompatibility tests, and helped writing the paper. C.-R. C. W. produced the molecular probes and helped writing the paper. C.-W. W. performed the imaging experiments and helped to write the paper. C. L. helped to build the imaging system. A. D. and Y. W. performed biocompatibility tests and helped to provide cells and animals. S. J. and C. P. helped to produce the molecular probes.

Methods

Cell culture

OECM1 cells were maintained in 90% RPMI1640 and 10% FBS (fetal bovine serum), and Cal27 cells were cultured in 90% DMEM and 10% FBS. All of the cell lines were maintained in a 37°C incubator with a humidified environment of 5% CO_2 in air.

Antibody production

HER2, EGFR, and CXCR4 antibodies was purchased from American Type Culture Collection (VA, USA), Thermo Fisher Scientific (MA, USA), and R&D Systems (MN, USA), respectively. HER2 antibodies were purified from the A-HER2 hybridoma (CRL-10463). Antibodies were produced and purified by GlycoNex (Taiwan).

Gold nanorods and nanoprobes

Gold nanorods were synthesized by the electrochemical conversion of an anodic gold material into particles within an electrolytic cosurfactant system, which is a procedure that we have developed previously[18, 19]. The cationic surfactants used were CTABr (hexadecyltrimethylammonium bromide) and TDABr (tetradodecylammonium bromide). The particle shape was successfully controlled using cationic cosurfactant micelles that included several other ingredients such as cyclohexane and trace amount of silver ions[20]. The gold nanorods were then well dispersed in aqueous solutions. Multiple-target studies were achieved using two nanorod samples and a gold-nanosphere system exhibiting surface plasmon resonances at approximately 800 and 1000 nm for the subsequent antibody conjugation and cell binding.

In addition to successful and stable conjugation of the recognition unit to the AuNRs through chemical bonding, it was also necessary that the nanoprobes exhibited high dispersity prior to binding to cancer cells. To achieve these goals, we adopted a conjugation protocol involving a 1-ethyl-3-(3-dimethylaminopropyl) carbodiimide hydrochloride (EDC-mediated coupling reaction and subsequent attachment of a blocking agent [mPEG-SH, a thiol-terminated methoxypoly (ethyleneglycol)] at nonspecific adsorption sites on the AuNRs[21, 22].

Briefly, the absorbance of a 1-ml aliquot of the AuNR solution was adjusted to 0.8, as measured under a 2-mm optical path length at the resonance. Five milliliters of 0.4 M cysteamine dihydrochloride and 10 ml of 16 mM HNO_3 were then added, and the solution was aged for 30 min before being centrifuged at 5500 rpm for 15 min and redispersed into 1 ml of deionized water to remove any excess cysteamine. In a separate vial, an EDC-mediated solution was prepared by adding 0.02 g of EDC to 100 μl of aqueous 1.04 M NHS (N-hydroxysuccinimide) solution and then aging the mixture for 10 min. A 2-ml aliquot of the EDC-mediated solution was mixed with 2 ml of a 8 mg/ml solution of HER2 monoclonal antibody (mAb) in 10 mM PBS in a microcentrifugation tube and then aged for 1 hour at 4 °C. To complete the conjugation process, this modified HER2 mAb solution was then added into the previously prepared cysteamine-modified AuNR solution (1 ml) and aged for 1 hour at 4 °C. This AuNR-HER2 mAb solution was flocculated by centrifugation at 5500 rpm for 15 min and then redispersed into 1 ml of aqueous 1.04 mM mPEG-SH (MW = 5000; Nektar) solution. The dispersed solution was then aged for either 1 hour or overnight. The final solution was again centrifuged at 5500 rpm for 15 min to remove any excess mPEG-SH. The flocculates were then redispersed into a 10 mM PBS solution to produce the nanoprobes. The aqueous nanoprobe solutions remained well dispersed for at least 1 month when stored at 4 °C.

Tumor induction in small animals

For *in vivo* studies, the cancer cells were induced on the back of NOD-scid male mice by the subcutaneous injection of 10^7 cells. The tumors were measured by the PA technique after 10–15 days of growth, and were typically 5 mm in diameter and 2–3 mm thick.

***In vivo* setup for PA measurements**

The optical irradiation was delivered by a widely tunable pulsed Ti:sapphire laser (CF-125, SOLAR TII, Minsk, Republic of Belarus) and an Nd:YAG laser lasing at 800 and 1064 nm, respectively. These wavelengths were chosen according to the peak absorptions of the gold nanoprobes. The pulse repetition rate was 10 Hz. A homemade PA transducer with a center frequency of 20 MHz and a focal depth of 9.5 mm was used for signal detection. The transducer was integrated with a single fiber (FT-600-UMT, Thorlabs, Newton, NJ) with a diameter of 600 μm through a hole at the center

of the transducer to achieve registered irradiation and detection. The integrated PA transducer was driven by a precision translation stage (HR8, Nanomotion, Yokneam, Israel) to perform one-dimensional cross-sectional scans of the tumor with a step size of 0.2 mm. The received acoustic waveforms were amplified by an ultrasonic receiver (5077PR, Panametrics, Waltham, MA) and then recorded at a sampling rate of 200 Msamples/second by a data acquisition card (CompuScope 14200, Gage, Lachine, QC, Canada).

Mice with tumor cells were anesthetized with halothane vapor using a vaporizer system (Fluosorber, Market Supply, UK), placed on a plate stage, and illuminated with an incandescent bulb to keep the mouse warm. Transparent ultrasonic gel (ECGEL 4000, Hometech, Taiwan) was added between the tumor region and the transducer to improve acoustic wave propagation. For mice with the OECM1 tumor, a 100-μl mixture of $AuNR_{785}$-HER2 and $AuNR_{785}$ at a concentration of 30 nM was prepared for injection, and the irradiating wavelength was 800 nm. For Cal27 tumors, a 100-μl mixture of $AuNR_{1000}$-EGFR and $AuNR_{1000}$ at a concentration of 30 nM was prepared for injection, and the irradiating wavelength was 1064 nm. For measurements of multiple targeting of OECM1 tumors, 50 μl of each of two nanoprobes ($AuNR_{785}$-HER2 and $AuNR_{785}$-CXCR4) were mixed at a concentration of 30 nM, and the irradiating wavelength was 800 nm.

References

1. Shah, K., Jacobs, A., Breakefield, X. O. and Weissleder, R. Molecular imaging of gene therapy for cancer. *Gene Ther.* **11**, 1175–1187 (2004).
2. Gao, X., Cui, Y., Levenson, R. M., Chung, L. W. K. and Nie, S. *In vivo* cancer targeting and imaging with semiconductor quantum dots. *Nat. Biotechnol.* **22**, 969–976 (2004).
3. Ellegala, D. B. 1st 3 *et al.* Imaging tumor angiogenesis with contrast ultrasound and microbubbles targeted to $\alpha_v\beta_3$. *Circulation* **108**, 336–341 (2003).
4. Josephson, L., Kircher, M. F., Mahmood, U., Tang, Y. and Weissleder, R. Near-infrared fluorescent nanoparticles as combined MR/optical imaging probes. *Bioconjug. Chem.* **13**, 554–560 (2002).
5. Cherry, S. R. *In vivo* molecular and genomic imaging: new challenges for imaging physics. *Phys. Med. Biol.* **49**, R13–R48 (2004).
6. Li, P. C. *et al.* Multiple targeting in photoacoustic imaging using bioconjugated gold nanorods. *Proc. SPIE* **6086**, 175–184 (2006).
7. Esenaliev, R. O., Karabutov, A. A. and Oraevsky, A. A. Sensitivity of laser opto-acoustic imaging in detection of small deeply embedded tumors. *IEEE J. Sel. Top. Quantum Electron.* **5**, 981–988 (1999).
8. Viator, J. A., Svaasand, L. O., Aguilar, G., Choi, B. and Nelson, J. S. Photoacoustic measurement of epidermal melanin. *Proc. SPIE* **4960**, 14–20 (2003).
9. Esenaliev, R. O. *et al.* Optoacoustic technique for noninvasive monitoring of blood oxygenation: a feasibility study. *Appl. Opt.* **41**, 4722–4731 (2002).
10. Wei, C. W., Huang, S. W., Wang, C. R. C. and Li, P. C. Photoacoustic flow measurements based on wash-in analysis of gold nanorods. *IEEE Trans. Ultrason. Ferroelectr. Freq. Control* **54**, 1131–1141 (2007).
11. Link, S. and El-Sayed, M. A. Spectral properties and relaxation dynamics for surface plasmon electronic oscillations in gold and silver nanodots and nanorods. *J. Phys. Chem. B* **103**, 8410–8426 (1999).
12. Fu, W. *et al.* Biomedical applications of gold nanoparticles functionalized using hetero-bifunctional poly (ethylene glycol) spacer. *Mater. Res. Soc. Symp. Proc.* **845**, AA5.4.1– AA5.4.6 (2005).

13. Meric-Bernstam, F. and Hung, M. C. Advances in targeting human epidermal growth factor receptor-2 signaling for cancer therapy. *Clin. Cancer Res.* **12**, 6326–6330 (2006).
14. Kalyankrishna, S. and Grandis, J. R. Epidermal growth factor receptor biology in head and neck cancer. *J. Clin. Oncol.* **24**, 2666–2672 (2006).
15. Hanaoka, H. *et al.* Development of a ^{111}In-labeled peptide derivative targeting a chemokine receptor, CXCR4, for imaging tumors. *Nucl. Med. Biol.* **33**, 489–494 (2006).
16. Hatse, S. *et al.* AMD3465, a monomacrocyclic CXCR4 antagonist and potent HIV entry inhibitor. *Biochem. Pharmacol.* **70**, 752–761 (2005).
17. Paciotti, G. F., Myer, L., Kingston, D. G. I., Ganesh, T. and Tamarkin, L. Colloidal gold nanoparticles: a versatile platform for developing tumor targeted cancer therapies. *NSTI-Nanotech.* **1**, 7–10 (2005).
18. Yu, Y. Y., Chang, S. S., Lee, C. L. and Wang, C. R. C. Gold nanorods: electrochemical synthesis and optical properties. *J. Phys. Chem. B* **101**, 6661–6664 (1997).
19. Chang, S. S., Shih, C. W., Chen, C. D., Lai, W. C. and Wang, C. R. C. The shape transition of gold nanorods. *Langmuir* **15**, 701–709 (1999).
20. Shih, C. W., Lai, W. C., Hwang, C. C., Chang, S. S. and Wang, C. R. C. *Metal Nanoparticles: Synthesis, Characterization, and Application in Preparation* (Marcel Dekker, Berkshire, UK, 2001).
21. Hirsch, L. R., Jackson, J. B., Lee, A., Halas, N. J. and West, J. L. A whole blood immunoassay using gold nanoshells. *Anal. Chem.* **75**, 2377–2381 (2003).
22. Liao, H. and Hafner, J. H. Gold nanorod bioconjugates. *Chem. Mater.* **17**, 4636–4641 (2005).

Figure Legends

Figure 1 Absorption spectra of gold nanorods with two aspect ratios: (A) $AuNR_{785}$ and (B) $AuNR_{1000}$.

Figure 2 Schematic diagram of the experimental setup for *in vivo* PA imaging.

Figure 3 Images of a Cal27 tumor before and after the injection of $AuNR_{1000}$ and $AuNR_{1000}$-EGFR. The ultrasound images are displayed on a grayscale, and the superimposed PA images obtained at **an optical wavelength of** 1064 nm are displayed in red pseudocolor. Ellipses indicate the tumor regions. (a) Control PA image before $AuNR_{1000}$ injection. (b) PA image at 7 hours after $AuNR_{1000}$ injection. (c) Control PA image before $AuNR_{1000}$-EGFR injection. (d) PA image at 7 hours after $AuNR_{1000}$-EGFR injection. (e) Averaged image intensities within the tumor region versus time for injections with $AuNR_{1000}$-EGFR (solid line) and $AuNR_{1000}$ (dashed line). The averages were calculated from three cross-sectional images. Error bars indicate standard deviations.

Figure 4 Images of an OECM1 tumor before and after the injection of $AuNR_{785}$ and a mixture of different probes ($AuNR_{785}$-HER2 and $AuNR_{785}$-CXCR4). The ultrasound images are displayed on a grayscale, and the superimposed PA images obtained at **an optical wavelength of** 800 nm are displayed in red pseudocolor. Ellipses indicate the tumor region. (a) Control PA image before $AuNR_{785}$ injection. (b) PA image at about 17 hours after $AuNR_{785}$ injection. (c) Control PA image before $AuNR_{785}$-HER2 injection. (d) PA image at about 17 hours after $AuNR_{785}$-HER injection. (e) Control PA image before injecting the mixture of different probes ($AuNR_{785}$-HER2 plus $AuNR_{785}$-CXCR4). (f) PA image at about 17 hours after mixed-probe injection. (g) Averaged image intensities within the tumor region versus time for injection with mixed probes (solid line), injection with $AuNR_{785}$-HER2 (dashed line), and injection with $AuNR_{785}$ (dotted line). The mean values were calculated from three cross-sectional images. Error bars indicate standard deviations.

Figure 5 Atomic absorption spectroscopy analysis of various organs taken from test mice at different time points after intravenous injections. Nanorods mainly accumulated in the spleen and liver, and they cleared after 168 hours.

Figure 6 Biodistributions of $AuNR_{785}$-HER2 and $AuNR_{785}$ from the organs removed at 24 hours postinjection. Data are mean and standard deviation values.

Figures

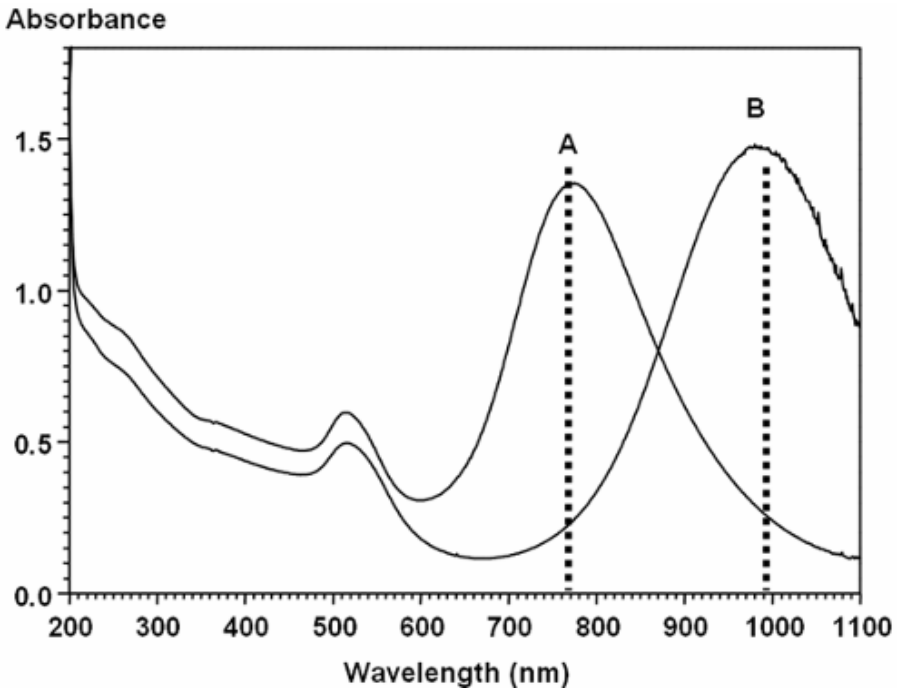

Figure 1

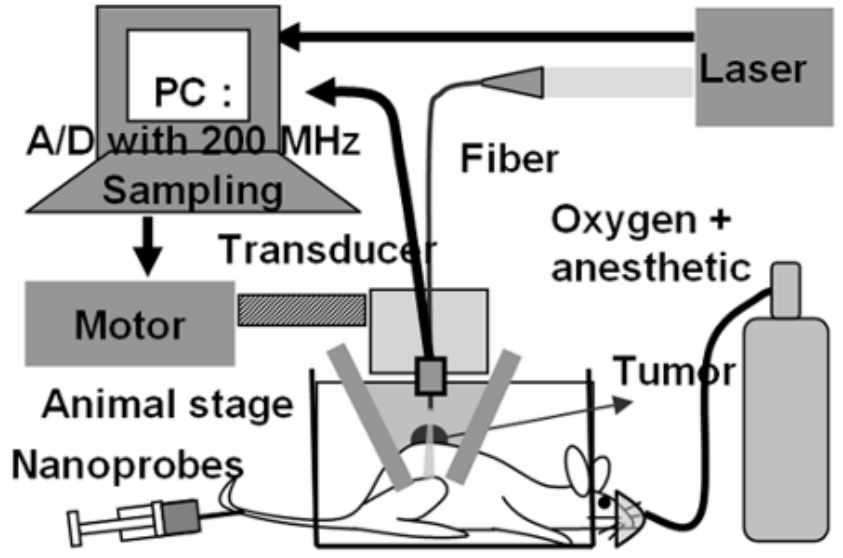

Figure 2

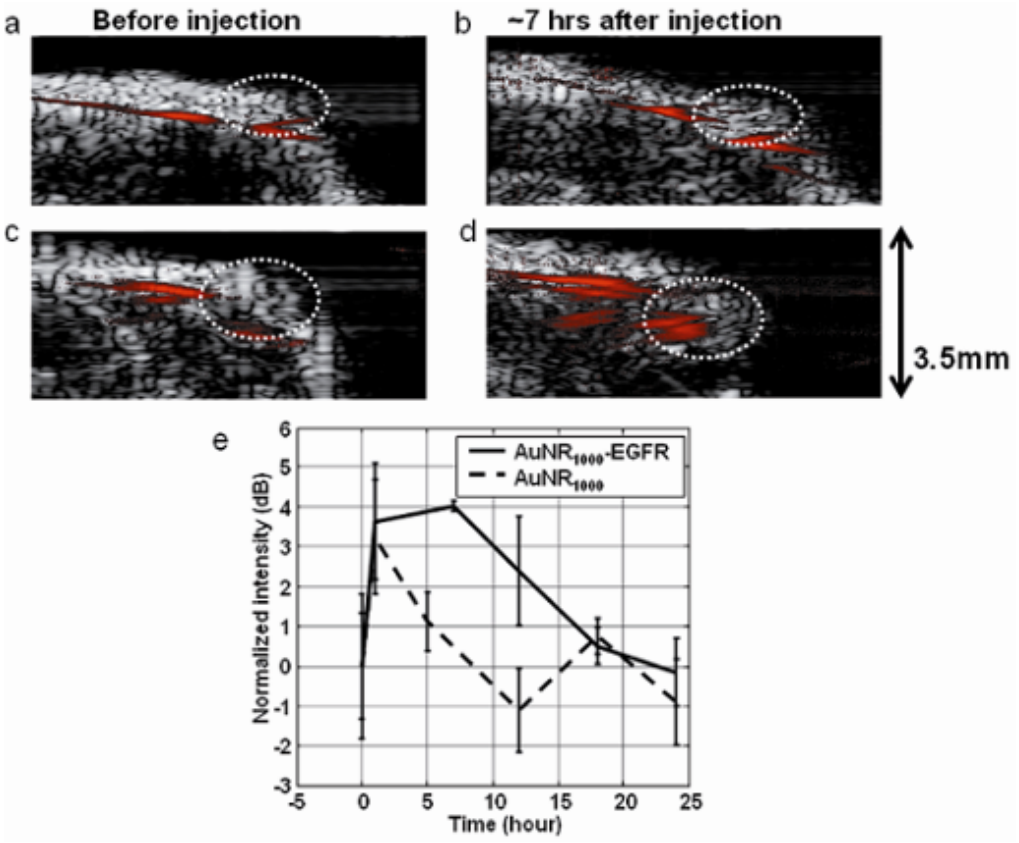

Figure 3

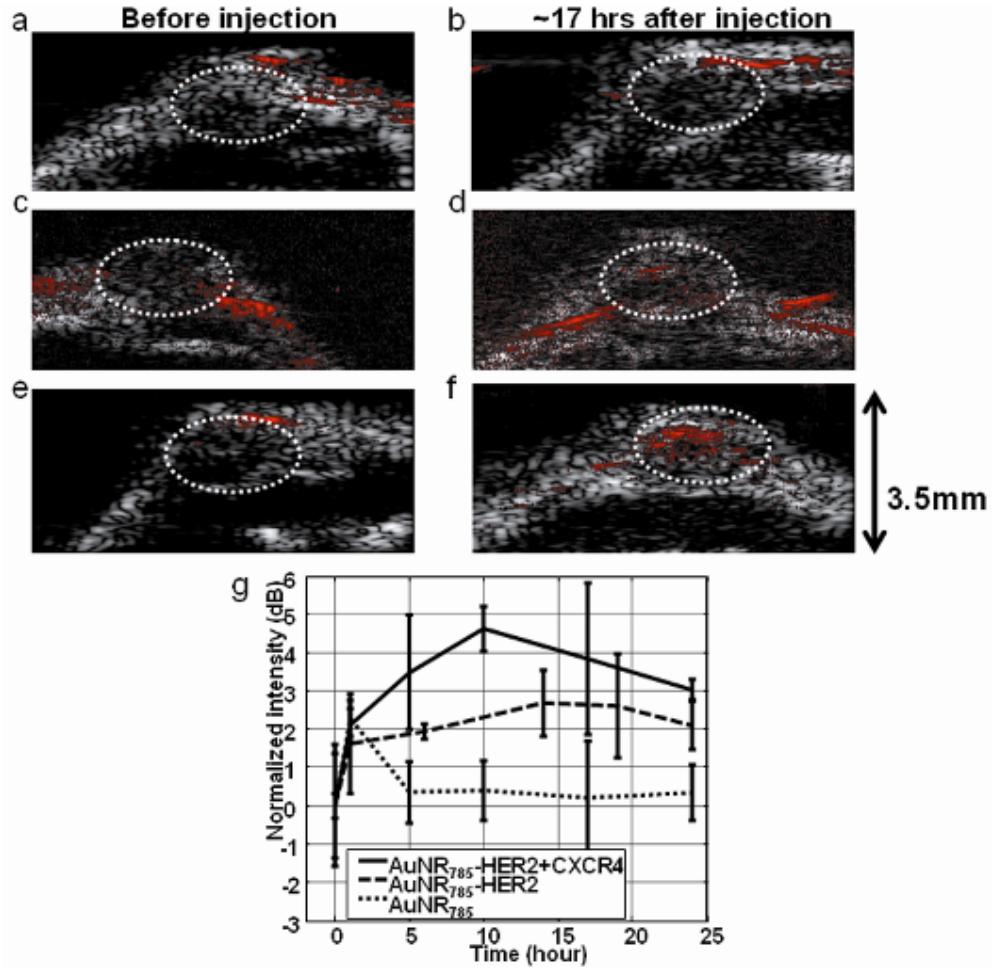

Figure 4

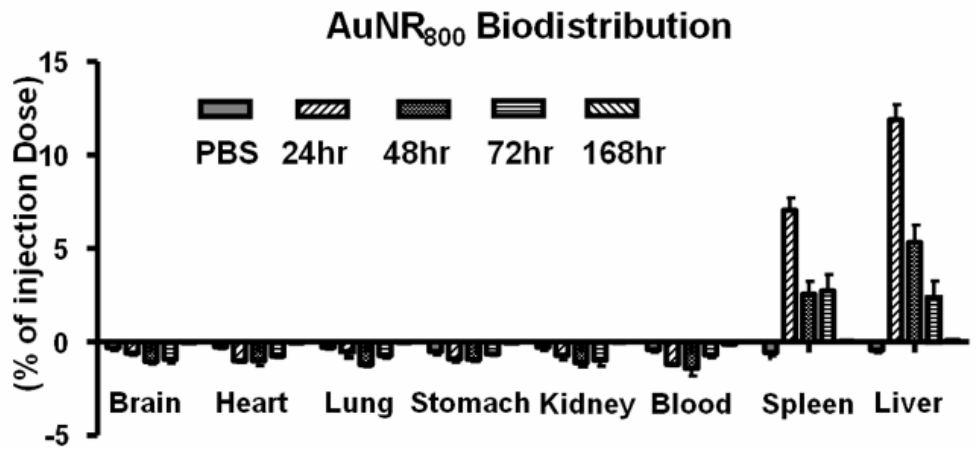

Figure 5

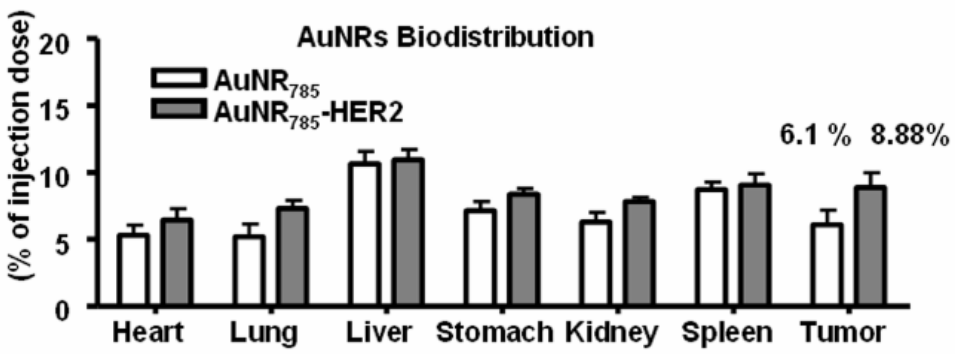

Figure 6